



Contents lists available at ScienceDirect

Journal of Quantitative Spectroscopy & Radiative Transfer

journal homepage: www.elsevier.com/locate/jqsrt

Air- and self-broadened half widths, pressure-induced shifts, and line mixing in the ν_2 band of $^{12}\text{CH}_4$

M.A.H. Smith^{a,*}, D. Chris Benner^b, A. Predoi-Cross^c, V. Malathy Devi^b^a Science Directorate, NASA Langley Research Center, Mail Stop 401A, Hampton, VA 23681-2199, USA^b Department of Physics, The College of William and Mary, Box 8795, Williamsburg, VA 23187-8795, USA^c Department of Physics, University of Lethbridge, 4401 University Drive, Lethbridge, Alberta, Canada, T1K 3M4

ARTICLE INFO

Article history:

Received 6 June 2013

Received in revised form

2 August 2013

Accepted 5 August 2013

Available online 14 August 2013

Keywords:

Methane

Infrared spectra

Fourier transform infrared (FTIR) spectroscopy

Spectral line shape

Pressure broadening

Pressure-induced shifts

Line mixing

Off-diagonal relaxation matrix elements

ABSTRACT

Lorentz self- and air-broadened half width and pressure-induced shift coefficients and their dependences on temperature have been measured from laboratory absorption spectra for nearly 130 transitions in the ν_2 band of $^{12}\text{CH}_4$. In addition line mixing coefficients (using the relaxation matrix element formalism) for both self- and air-broadening were experimentally determined for the first time for a small number of transitions in this band. Accurate line positions and absolute line intensities were also determined. These parameters were obtained by analyzing high-resolution (~ 0.003 to 0.01 cm^{-1}) laboratory spectra of high-purity natural CH_4 and air-broadened CH_4 recorded at temperatures between 226 and 297 K using the McMath–Pierce Fourier transform spectrometer (FTS) located at the National Solar Observatory on Kitt Peak, Arizona. A multispectrum nonlinear least squares technique was used to fit short ($5\text{--}15\text{ cm}^{-1}$) spectral intervals in 24–29 spectra simultaneously. Parameters were determined for ν_2 transitions up to $J'' = 16$. The variations of the measured broadening and shift parameters with the rotational quantum number index and tetrahedral symmetry species are examined. The present results are also compared with previous measurements available in the literature.

Published by Elsevier Ltd.

1. Introduction

Accurate knowledge of pressure-broadened half width and pressure-induced line shift coefficients of methane is very important for the interpretation and modeling of infrared spectroscopic observations in many remote sensing studies involving the terrestrial and planetary atmospheres. In addition to measurements of these coefficients at room temperature, low temperature measurements of the same parameters are needed to aid in interpreting measurements of Earth's upper atmosphere and the atmospheres of other planets. The transitions of the normally

infrared inactive ν_2 fundamental band appear in the infrared because of the Coriolis interaction with the ν_4 band. With sufficient optical densities in the spectra these transitions acquire enough strength to be measured and interpreted. Along with the ν_4 band, the ν_2 band has some importance in radiative transfer calculations of planetary atmospheres having high concentrations of methane (e.g., the giant planets and Saturn's moon Titan), and accurate knowledge of spectroscopic parameters of the ν_2 transitions will improve these calculations.

Pressure broadening coefficients in the infrared spectra of methane have been the subject of numerous experimental and theoretical studies. Numerous transitions in several methane bands with different broadening gases (such as CH_4 , air, Ar, N_2 , O_2) have been studied during the past few decades (see Refs. [1–9] and the references cited

* Corresponding author. Tel.: +1 757 864 2701; fax: +1 757 864 4344.
E-mail address: MaryAnn.H.Smith@nasa.gov (M.A.H. Smith).

therein). The number of laboratory studies focusing on pressure-induced shift coefficients has been limited in the past because (1) pressure-induced shifts of methane, being much smaller than the line widths, were thought to not significantly affect remote sensing retrievals and (2) the measurement of pressure-induced shifts requires accurate calibration of numerous laboratory spectra to the same wavenumber scale. However, in recent years the pressure-induced shift coefficients in several different methane bands have been investigated with high precision and accuracy due to the development of high-resolution recording instruments such as Fourier transform spectrometer (FTS), tunable diode laser spectrometers, and difference frequency laser spectrometers and the availability of sophisticated analysis techniques (see Refs. [1–6,10–13]). Information on line shape parameters including speed dependence and line mixing is also becoming available as advanced analysis techniques are applied to high-resolution, high signal-to-noise spectra [11,12,14–16]. However, most of the previous studies of methane line broadening and shift parameters have focused on the stronger fundamental bands such as ν_4 and ν_3 .

For transitions in the ν_2 $^{12}\text{CH}_4$ band, the first high-resolution experimental values of self-, air- and N_2 -broadened Lorentz half width and pressure-induced shift coefficients were reported for five transitions measured with a tunable diode laser by Malathy Devi et al. [17]. Later measurements with Fourier transform spectrometers resulted in air- and N_2 -broadened Lorentz half width and pressure-induced shift coefficients for 47 transitions [18] and helium and argon-broadened half width coefficients for about 100 transitions [19]. All of these measurements were made at room temperature. Several recent studies [20–22] have examined line mixing in the fundamental bands, including ν_2 [20], using experimental spectra at pressures of tens to hundreds of atmospheres, and measurements of line mixing at terrestrial atmospheric pressures have been reported in the ν_4 bands of $^{12}\text{CH}_4$ [1,2] and $^{13}\text{CH}_4$ [3] and in the ν_3 [6,11,23–26] and $\nu_2 + \nu_3$ [16] bands of $^{12}\text{CH}_4$.

In this article we report measurements of line positions, absolute line intensities and self- and air-broadened

half width coefficients and pressure-induced shift coefficients for 154 transitions in the $^{12}\text{CH}_4$ ν_2 band. This work includes the first experimental determination of temperature dependences of most of these half widths and shifts over the range from 226 to 297 K. We also report experimentally determined off-diagonal relaxation matrix element (ORME) coefficients for line mixing between 10 pairs of transitions in this band. For brevity in the following discussion of this paper, we will use the acronym ORME for off-diagonal relaxation matrix element(s).

2. Experiment and data retrievals

The 29 spectra used in the present analysis of the $^{12}\text{CH}_4$ ν_2 band are a subset of the larger group of 64 spectra used for the determination of air- and self-broadening, shift, and line mixing parameters in the stronger ν_4 band of $^{12}\text{CH}_4$ [1,2] and in the ν_4 band of $^{13}\text{CH}_4$ [3]. All of the spectra were recorded using the one-meter McMath–Pierce Fourier transform spectrometer at the National Solar Observatory (NSO) on Kitt Peak, Arizona. For the analysis of the ν_2 band, which is much weaker than the ν_4 , we selected only those spectra in which the ν_2 signal was significant, i.e., those with larger volume mixing ratios or longer path lengths. Thus the data set of air-broadened spectra includes four spectra recorded with a 1.5 m stainless steel cell [18] and about 3% volume mixing ratio at room temperature (~ 297 K), as well as 15 low-temperature spectra recorded with the 50-cm coolable cell [27] and methane–air volume mixing ratios between 16% and 35%. For safety, the maximum total sample pressures for both air-broadening and self-broadening were kept below local atmospheric pressure (~ 650 Torr). The lowest gas sample temperatures were about 226 K for self-broadening and 233 K for air-broadening. The experimental conditions of the spectra analyzed in this work are listed in Table 1.

The experimental procedures for recording the spectra have been described in detail previously [1,2,18,27], and they are briefly summarized here. The unapodized resolutions of the spectra were ~ 0.003 – 0.01 cm^{-1} . Research-grade natural methane samples and commercially-supplied dry air were used to record the self-broadened and the air-broadened

Table 1
Summary of experimental conditions of the CH_4 spectra used to fit the ν_2 transitions.

Temperature (K)	Gas mixture	CH_4 volume mixing ratio	Path (m)	Pressure range (Torr)	Number of spectra
295.8	CH_4	1.	1.50	1.18	1
297.4–297.5	CH_4 in air	0.0272–0.0275	1.50	199.6–425.0	4
292.4	CH_4	1.	0.50	11.0	1 ^a
293.5–295.9	CH_4 in air	0.16–0.30	0.50	140.2–520.1	5 ^b
272.5	CH_4	1.	0.50	301.0	1
272.4–272.5	CH_4 in air	0.33	0.50	177.0–452.8	3
253.9–254.4	CH_4	1.0	0.50	209.0–645.0	3
253.8	CH_4 in air	0.304	0.50	229.1–509.2	2
240.7–240.8	CH_4 in air	0.30–0.35	0.50	99.2–328.2	3
232.7–232.8	CH_4	1.0	0.50	128.5–370.5	3
232.6	CH_4 in air	0.31	0.50	418.6	2
225.9	CH_4	1.0	0.50	643.0	1

Note: 760 Torr = 1 atm = 101.325 kPa.

^a Temperature erroneously listed as 254.0 K in Refs. [1–3].

^b Temperature range erroneously listed as 252.9–250.5 K in Refs. [1–3].

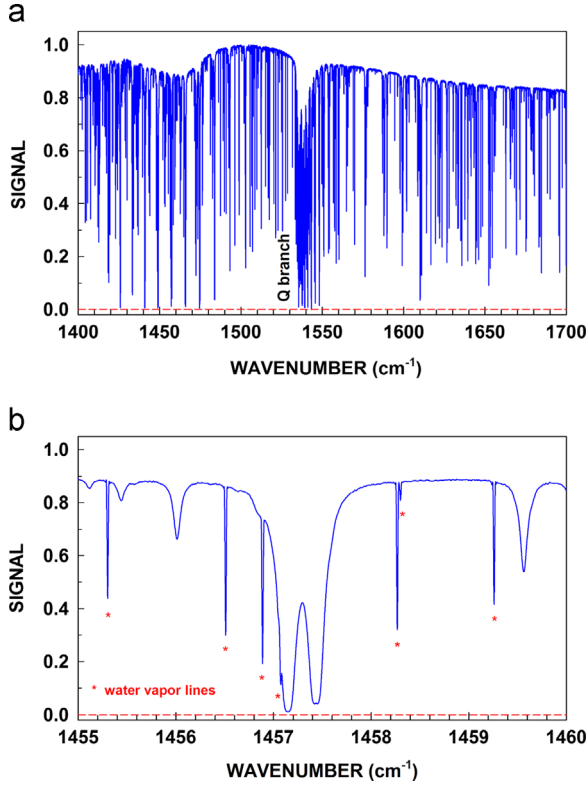


Fig. 1. (a) Methane spectrum in the ν_2 spectral region. The spectrum shown is self-broadened with ~ 305 Torr of pure natural methane at 233.2 K in a 50-cm absorption cell. (b) A short spectral interval 5 cm^{-1} wide from (a) around 1457 cm^{-1} is re-plotted to illustrate the presence of water vapor ν_2 band transitions (marked with an *). The dashed horizontal line in each panel corresponds to 100% absorption.

spectra. Gas sample pressures and temperatures were continuously monitored during the 1 to 1.5-h recording period for each spectrum using thermistor probes or thermocouples attached to the outside cell walls. The source of radiation was a glower operating at 110 V. Two optical filters (CaF_2 and InAs), a KCl beam splitter, and helium-cooled As:Si detectors were used in the experimental set up. The useful wavenumber coverage of each spectrum was approximately $800\text{--}2800 \text{ cm}^{-1}$. Signal to noise ratios in some of the spectra were as high as 1000:1 in the region of the $^{12}\text{CH}_4$ ν_2 band.

A methane spectrum covering the entire ν_2 band is displayed in Fig. 1(a). The spectrum was obtained using the 50-cm coolable cell containing 305 Torr of a pure natural-abundance methane sample at 233.2 K. In the lower panel (b) a short interval around 1457 cm^{-1} from the same spectrum is expanded to illustrate the presence of strong water vapor ν_2 band lines that appear along with the methane absorption features in most of the spectra analyzed. These transitions arise from residual water vapor in the “evacuated” spectrometer tank that encloses the FTS and also from the nitrogen-purged segments of the optical path outside the sample cell between the glower source and the entrance aperture of the FTS. Interference from these water vapor lines posed great difficulties in fitting the spectra simultaneously. In order to fit all the spectra at the same time, the amount of water present in each spectrum had to

be known precisely. The different amounts of water absorption from one spectrum to another, together with the fact that the amount of water in the optical path also slightly varied during the recording of each spectrum, made it difficult to achieve good fits of spectral regions containing these water vapor transitions.

Details about the calibration of the wavenumber scales of the spectra have been given in several previous papers [1,18,27]. Briefly, the calibration correction factor applied to each spectrum was determined from averaging the differences in measured positions of at least 20 ν_2 water vapor transitions relative to those reported in Ref. [28]. With this calibration method we estimate that the absolute accuracies for the measured line positions of isolated CH_4 ν_2 transitions are within $\pm 0.0001 \text{ cm}^{-1}$.

As in our recent analyses of air- and self-broadened spectra in the ν_4 bands of $^{12}\text{CH}_4$ and $^{13}\text{CH}_4$ [1–3], an interactive multispectrum nonlinear least squares technique [10] was used to fit short spectral intervals ($5\text{--}15 \text{ cm}^{-1}$) of 24–29 spectra simultaneously, depending upon the spectral region. The relationships between the air- and self-broadened half width and pressure-induced shift coefficients and their temperature dependences, and the terminology used in our multispectrum nonlinear least squares fitting algorithm are given in Refs. [1–3]. Eqs. (1)–(3) are repeated here for the convenience of the reader.

$$b_L(p, T) = p \times \left[b_L^0(\text{air})(p_0, T_0) \times (1-\chi) \times \left[\frac{T_0}{T} \right]^{n_1} + b_L^0(\text{self})(p_0, T_0) \times \chi \times \left[\frac{T_0}{T} \right]^{n_2} \right] \quad (1)$$

$$\nu = \nu_0 + p \times [\delta^0(\text{air}) \times (1-\chi) + \delta^0(\text{self}) \times \chi] \quad (2)$$

$$\delta^0(T) = \delta^0(T_0) + \delta' \times (T - T_0) \quad (3)$$

In Eq. (1) $b_L(p, T)$ is the Lorentz half width (in cm^{-1}) of the spectral line at pressure p and temperature T , and $b_L^0(\text{Gas})(p_0, T_0)$ is the Lorentz half width coefficient of the line at the reference pressure p_0 (1 atm) and temperature T_0 (296 K) of the broadening gas (either air or methane), and χ is the ratio of the partial pressure of methane to the total sample pressure in the cell. The temperature dependence exponents of the pressure-broadened half width coefficients (air- and self-) are represented by n_1 and n_2 , respectively. In Eq. (2), ν_0 is the zero-pressure line position (in cm^{-1}), ν is the line position (in cm^{-1}) corresponding to the pressure p and temperature T , $\delta^0(\text{Gas})$ is the pressure-induced shift coefficient in $\text{cm}^{-1} \text{ atm}^{-1}$ at T , and χ has the same meaning as in Eq. (1). In Eq. (3) δ' represents the temperature dependence of the pressure-induced shift coefficients, and $\delta^0(T)$ and $\delta^0(T_0)$ represent the pressure-induced shift coefficients (in $\text{cm}^{-1} \text{ atm}^{-1}$) at temperatures T and T_0 (296 K), respectively.

As in our previous analyses of the ν_4 bands of $^{12}\text{CH}_4$ and $^{13}\text{CH}_4$ [1–3], initial values for all line parameters (e.g., positions, intensities, lower state energies, half width coefficients) were taken from the HITRAN04 database [29]. Initial values of self-shift coefficients were set to zero. Similarly, initial values of the temperature dependence exponents of self-broadened half width coefficients were assumed to be 0.7 for all transitions. The air- and

self-shift coefficients of all unmeasured transitions were fixed to $-0.002 \text{ cm}^{-1} \text{ atm}^{-1}$ at T (T =temperature of the sample). The temperature dependence exponents of air- and self-broadened half width coefficients for all unmeasured lines were held fixed to the default value of 0.7. An initial estimate of zero was assumed for δ' for both air- and self-shift coefficients. The temperature dependence coefficients of air- and self-shifts for transitions whose parameters were not adjusted in the least squares fits remained fixed at zero.

A modified Voigt line shape that included speed dependence ([6] and references cited therein) and line mixing (via the full relaxation matrix formulation [30]) was used to retrieve the various line parameters. The optical densities of the spectra available for the present analysis were not high enough to measure the line mixing coefficients in many of the P- and R-manifolds of the ν_2 band. However, in some cases it was necessary to include line mixing to fit the data to the noise level. Since the total pressures of nearly all of our spectra (see Table 1) were higher than the pressure range typically used for high-precision laboratory studies of collisional narrowing in methane (e.g., Refs. [23,26,31–33]), we expected any collisional narrowing to be masked by Lorentzian pressure broadening [23]. Initial test fits showed that solving for speed dependence or Dicke narrowing parameters in the data analysis did not improve the fit residuals significantly in any spectral interval of the ν_2 band, and therefore these parameters could not be uniquely determined from our set of FTS spectra. Therefore, the final broadening, shift, and line mixing parameters were determined with the speed dependence and Dicke narrowing parameters held fixed to default values of zero. In the multispectrum fitting procedure, in addition to the various spectral line parameters that were adjusted during the least squares solutions, spectral backgrounds (including some channel spectra), zero transmission levels, residual FTS phase errors and FTS instrument line shapes were also modeled appropriately [1,18,34].

Examples of two fitted intervals where line mixing was not required to fit the data well within the noise level, and one interval where inclusion of line mixing was necessary, are shown in Figs. 2–4. In all three figures, the red curves represent self-broadened methane spectra, the blue curves denote air-broadened spectra, and tick marks at the top of the uppermost panel indicate the positions of all lines included in the fits.

Fig. 2 shows the observed spectra and weighted residuals from a simultaneous fit of 28 air- and self-broadened methane spectra in the P(8) manifold. Five transitions in the ν_2 P(8) manifold are seen in this interval from 1452.3 to 1454.2 cm^{-1} , which also includes the R(9) F2 7←F1 1 transition of the ν_4 band (marked with an asterisk). This interval could be fit with all 28 spectra using the standard Voigt line shape without line mixing.

Fig. 3 shows a simultaneous fit of air- and self-broadened spectra in the ν_2 R(7) manifold, where the transition strengths are comparable to those in the P(8) manifold. All 29 experimental spectra are shown in the top panel (a); the weighted fit residuals with the standard Voigt profile are shown in middle panel (b); and in the bottom panel (c) the weighted residuals resulting from

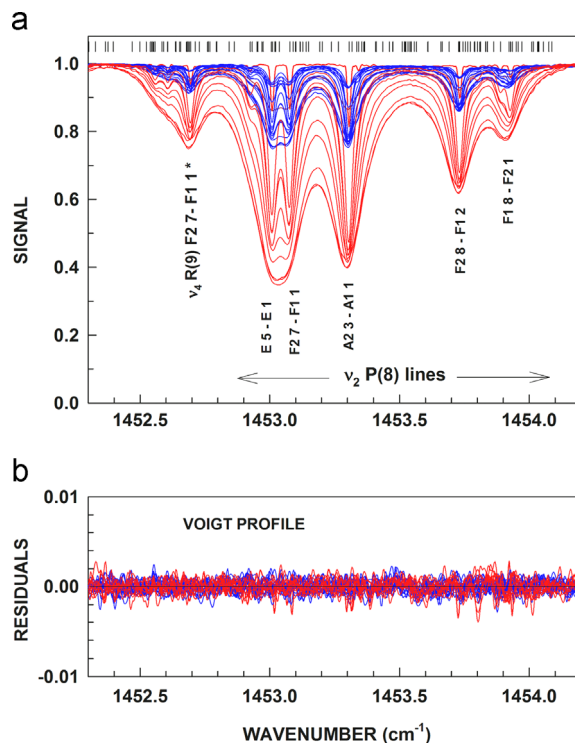


Fig. 2. Multispectrum fit of 28 self- and air-broadened methane spectra in the P(8) manifold. (a) Observed spectra. Tick marks at the top of the panel indicate the positions of all spectral lines included in the fit, and identifications are given for methane lines for which parameters were determined in the fits. (b) Weighted residuals of the fit using the standard Voigt line shape. In both panels, red curves indicate self-broadened spectra and blue curves indicate air-broadened spectra. No line mixing was necessary to fit all of the spectra to their noise levels. (For interpretation of the references to color in this figure legend, the reader is referred to the web version of this article.)

including line mixing (Voigt profile with ORME) in the multispectrum fit are plotted. The residuals shown in the lower panels of Fig. 3 indicate that in this case it was necessary to include line mixing in order to fit the observed spectra to their noise levels. The ORME for mixing between the R(7) F2 9←F1 2 and F1 9←F2 2 transitions was determined from this fit.

In Fig. 4 we show a multispectrum fit of 26 air- and self-broadened spectra in a high- J manifold, P(14). The transitions in this region are weaker than those in the mid- J manifolds shown in the two previous figures. The strong overlap of the P(14) lines in most of the pressure-broadened spectra is obvious in the top panel (a); without the multispectrum fitting technique it would not have been possible to fit some of these spectra. Although there are two pairs of F-species P(14) transitions that could be involved in mixing, it was not necessary to include line mixing to fit all 26 spectra within their noise levels. A weak ν_2 water vapor transition overlaps the methane ν_2 P(14) manifold. For reasons explained earlier, this water line could not be fit very well. However, this situation does not affect the overall fit of methane transitions. A methane ν_4 transition, R(6) E 3←E 1, indicated with an asterisk in the figure, also appears in this spectral interval.

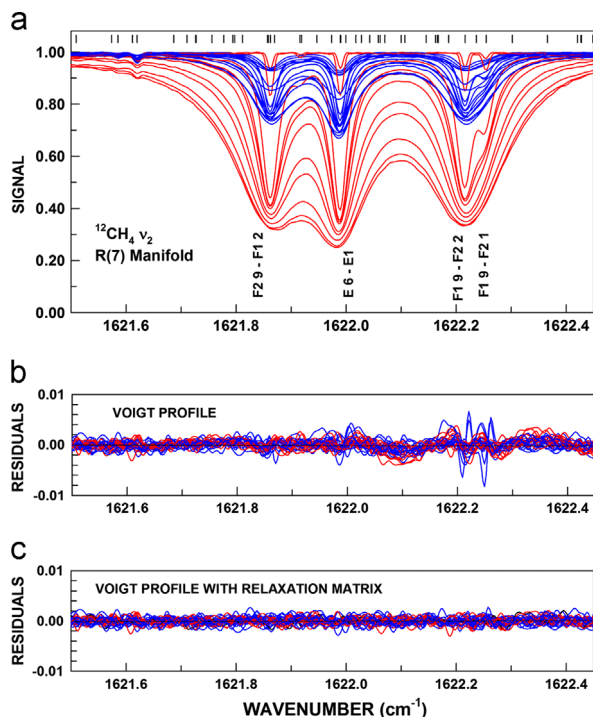


Fig. 3. Multispectrum fit of 29 self- and air-broadened methane spectra in the R(7) region. (a) Observed spectra. (b) Weighted residuals of the fit using the standard Voigt line shape with no modification. (c) Weighted residuals of the fit with Voigt line shape modified with the full relaxation matrix formulation for line mixing. The meaning of the tick marks and colored curves is the same as in Fig. 2. (For interpretation of the references to color in this figure legend, the reader is referred to the web version of this article.)

3. Results and discussion

The results from the present analysis are listed in Table 2. An ASCII text version of this table is available as a Supplemental file. The first few columns in Table 2 list the upper and lower state vibrational quantum numbers of each transition, followed by the measured line positions, absolute line intensities, pressure-broadened half width coefficients, their temperature dependence exponents, pressure-induced shift coefficients and their temperature dependence coefficients. The uncertainties associated with each of the measured parameters are also listed next to the appropriate quantities. In the case of line intensities the measurement uncertainties are given in percent, whereas for other parameters, the errors are given in the units of the measured value in parentheses following the measured values. In all cases, the uncertainties correspond to one sigma standard deviation in the measured quantities in the last quoted digit(s). For each transition the results for self-broadened widths and self-shift coefficients and their temperature dependences are listed below the corresponding values for air broadening. Shift coefficients and their temperature dependences are presented only for those transitions for which the corresponding widths and temperature dependences were also determined. Complete sets of air- and self-broadened widths, shifts and temperature dependences were retrieved for 127 of the 154

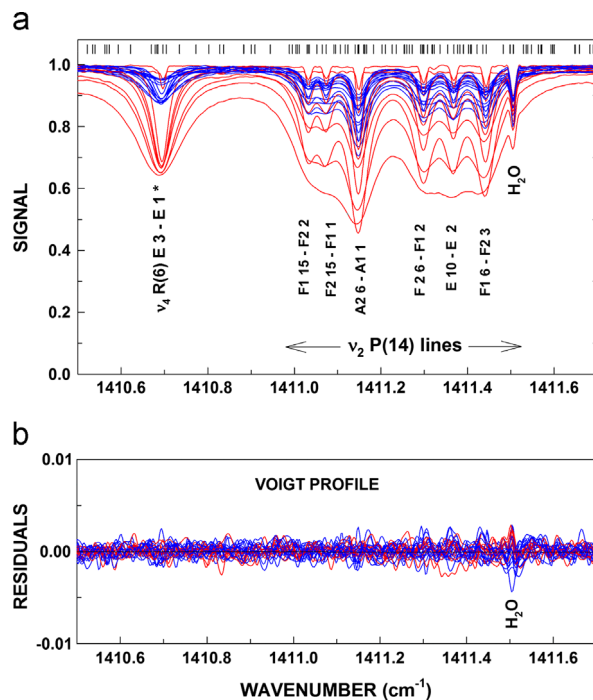


Fig. 4. Multispectrum fit of 26 self- and air-broadened methane spectra in the P(14) manifold. (a) Observed spectra. (b) Weighted residuals of the fit using the standard Voigt line shape. No line mixing was necessary to fit this region to the noise levels of the spectra. The R(6) E-transition of the ν_4 band is marked with an asterisk, and a contaminant water vapor transition near 1411.5 cm^{-1} is also marked. The meaning of the tick marks and colored curves is the same as in Figs. 2 and 3. (For interpretation of the references to color in this figure legend, the reader is referred to the web version of this article.)

transitions listed in Table 2. Missing parameters are generally associated with weak or blended lines.

As discussed in Ref. [1] the estimation of absolute uncertainties due to errors in the measurement of experimental conditions, errors in the line parameters assumed for unmeasured transitions, and other factors, is not trivial. Nevertheless, we estimate that the absolute uncertainties in our measured parameters for ν_2 are comparable to those for ν_4 [1,2]; 1% for half width coefficients, 10–15% for pressure-induced shift coefficients, 10% for n_1 and n_2 , and 20–50% for the temperature dependence coefficients of the pressure-induced shifts (δ'), added to the statistical uncertainties listed in Table 2. The statistical uncertainties in the measured width coefficients are less than 1% for the strong unblended lines and less than 10% for most of the weaker high J transitions. Statistical uncertainties for the other measured ν_2 parameters (shifts, temperature dependences) are somewhat larger.

Although the major thrust of the present analysis was to derive accurate values for pressure-broadened half width and shift coefficients and their temperature dependences, we were also able to retrieve accurate values of line positions and intensities. Positions and intensities obtained for $^{12}\text{CH}_4 \nu_2$ lines in this study are in excellent agreement with values listed in the HITRAN04 [29], the HITRAN08 [35] and the HITRAN 2012 [9,36] databases. For the 154 lines whose measurements are reported in this

Table 2
Measured spectral line parameters for air- and self-broadening in the methane ν_2 band sorted by lml .

lml	ΔJ	J'	C'	n'	J''	C''	n''	Position ^a	Intensity ^b	% unc	Broadening gas	Width ^c	Width temp dependence ^d	Shift ^e	Shift temp dependence ^e
3	R	3	F1	4	2	F2	1	1565.48185(3)	6.251E-23	0.08	Air Self	0.0700(2) 0.0692(1)	1.02(2) 0.71(1)	-0.00148(25) -0.00264(13)	+0.000004(7) -0.000006(3)
3	R	3	E	3	2	E	1	1565.82257(4)	3.596E-23	0.10	Air Self	0.0735(3) 0.0739(1)	1.06(3) 0.70(1)	-0.00292(37) -0.00195(17)	-0.000003(10) +0.000031(3)
3	P	2	F2	3	3	F1	1	1502.23987(8)	1.486E-23	0.30	Air Self	0.0719(7) 0.0710(3)	0.97(7) 0.74(2)	-0.00640(77) -0.00654(34)	+0.000017(21) +0.000016(7)
3	P	2	F1	3	3	F2	1	1502.60757(2)	7.369E-23	0.08	Air Self	0.0684(2) 0.0706(1)	0.95(2) 0.62(1)	-0.00350(18) -0.00523(12)	+0.000021(5) +0.000012(2)
3	P	2	A1	2	3	A2	1	1502.82425(2)	2.419E-22	0.07	Air Self	0.0722(1) 0.0770(2)	1.02(1) 0.59(1)	-0.00231(14) -0.00400(14)	+0.000013(4) +0.000008(3)
4	R	4	F1	5	3	F2	1	1576.77372(2)	9.683E-23	0.09	Air Self	0.0658(1) 0.0713(1)	0.99(1) 0.60(1)	-0.00131(16) -0.00127(14)	+0.000002(4) +0.000015(3)
4	R	4	F2	5	3	F1	1	1577.00596(3)	7.392E-23	0.09	Air Self	0.0720(2) 0.0742(1)	0.95(2) 0.65(1)	-0.00701(20) -0.00473(14)	+0.000013(5) +0.000042(3)
4	R	4	F2	6	3	F1	1	1578.05555(7)	2.046E-23	0.20	Air Self	0.0698(6) 0.0714(3)	0.85(5) 0.62(2)	-0.00113(58) -0.00297(30)	+0.000024(14) -0.000002(6)
4	P	3	E	3	4	E	1	1492.48876(2)	7.732E-23	0.08	Air Self	0.0702(1) 0.0731(1)	0.96(1) 0.63(1)	-0.00349(17) -0.00431(11)	+0.000042(4) +0.000029(2)
4	P	3	F2	4	4	F1	1	1492.67959(4)	5.025E-23	0.14	Air Self	0.0723(3) 0.0721(1)	1.06(3) 0.68(1)	-0.00395(33) -0.00430(22)	+0.000028(9) +0.000018(4)
4	P	3	F1	5	4	F2	1	1493.18052(1)	2.523E-22	0.04	Air Self	0.0708(1) 0.0749(1)	1.01(1) 0.53(1)	-0.00305(8) -0.00312(7)	-0.000009(2) +0.000010(1)
5	R	5	F1	5	4	F2	1	1586.94595(2)	7.319E-23	0.06	Air Self	0.0726(2) 0.0744(1)	0.97(2) 0.63(1)	+0.00444(18) +0.00036(11)	-0.000011(5) -0.000016(2)
5	R	5	F1	6	4	F2	1	1587.83315(2)	1.402E-22	0.04	Air Self	0.0637(1) 0.0686(1)	0.96(1) 0.57(1)	-0.00084(10) -0.00165(7)	-0.000016(3) -0.000002(2)
5	R	5	E	4	4	E	1	1588.03036(2)	1.054E-22	0.05	Air Self	0.0605(1) 0.0670(1)	0.99(1) 0.56(1)	-0.00411(11) -0.00422(8)	+0.000033(3) +0.000021(2)
5	R	5	F2	6	4	F1	1	1588.32762(2)	9.233E-23	0.05	Air Self	0.0707(1) 0.0734(1)	1.10(1) 0.61(1)	-0.00580(15) -0.00574(9)	+0.000035(4) +0.000021(2)
5	R	5	A2	3	4	A1	1	1589.73312(1)	1.798E-22	0.05	Air Self	0.0704(1) 0.0756(1)	1.10(1) 0.56(1)	-0.00488(11) -0.00548(8)	+0.000041(3) +0.000023(2)
5	R	5	F2	7	4	F1	1	1589.85711(5)	3.395E-23	0.13	Air Self	0.0678(3) 0.0721(2)	1.13(3) 0.61(2)	-0.00345(36) -0.00292(23)	+0.000026(10) +0.000021(5)
5	P	4	F1	5	5	F2	1	1482.52285(2)	1.177E-22	0.06	Air Self	0.0727(1) 0.0728(1)	1.00(1) 0.69(1)	-0.00656(13) -0.00684(10)	+0.000040(3) +0.000019(2)
5	P	4	F2	6	5	F1	2	1483.79236(1)	3.546E-22	0.09	Air Self	0.0681(1) 0.0755(2)	1.10(1) 0.49(1)	-0.00031(10) -0.00474(16)	+0.000007(3) -0.000025(3)
5	P	4	E	4	5	E	1	1483.83445(2)	2.245E-22	0.12	Air Self	0.0658(1) 0.0704(2)	1.02(1) 0.57(1)	-0.00032(13) -0.00028(19)	+0.000004(3) +0.000008(4)
6	R	6	F2	6	5	F1	2	1597.74628(6)	4.186E-23	0.41	Air Self	0.0720(5) 0.0729(4)	0.90(5) 0.54(2)	+0.00503(56) +0.00325(39)	-0.000039(14) -0.000025(7)
6	R	6	E	4	5	E	1	1597.77031(5)	5.816E-23	0.29	Air Self	0.0712(4) 0.0743(2)	1.18(4) 0.65(2)	+0.00015(40) -0.00079(30)	-0.000046(11) -0.000022(6)

6	R	6	F2	7	5	F1	2	1599.01101(1)	2.115E-22	0.05	Air	0.0629(1)	1.12(1)	-0.00071(8)	-0.000008(2)
											Self	0.0701(1)	0.52(1)	-0.00150(7)	+0.000012(1)
6	R	6	E	5	5	E	1	1599.41395(2)	9.318E-23	0.06	Air	0.0585(1)	1.06(1)	-0.00263(2)	+0.000011(3)
											Self	0.0644(1)	0.58(1)	-0.00371(9)	+0.000008(2)
6	R	6	F1	7	5	F2	1	1599.55939(2)	1.455E-22	0.05	Air	0.0665(1)	1.10(1)	-0.00412(11)	+0.000035(3)
											Self	0.0717(1)	0.61(1)	-0.00474(8)	+0.000027(2)
6	R	6	F2	8	5	F1	1	1601.76710(2)	1.176E-22	0.05	Air	0.0698(1)	1.09(1)	-0.00626(12)	+0.000012(3)
											Self	0.0731(1)	0.60(1)	-0.00541(8)	+0.000033(2)
6	R	6	E	6	5	E	1	1601.94255(13)	1.450E-23	0.46	Air	0.0798(11)	0.92(9)	-0.00163(117)	+0.000042(31)
											Self	0.0757(5)	0.72(4)	+0.00137(63)	+0.000011(12)
6	R	6	F1	8	5	F2	1	1601.98985(13)	1.289E-23	0.47	Air	0.0679(10)	0.97(10)	-0.00382(107)	+0.000089(29)
											Self	0.0687(5)	0.65(4)	+0.00028(60)	+0.000060(11)
6	P	5	A2	3	6	A1	1	1474.56079(1)	9.256E-22	0.06	Air	0.0631(1)	1.15(1)	-0.00069(5)	+0.000005(1)
											Self	0.0748(1)	0.38(1)	-0.00358(12)	+0.000011(2)
6	P	5	F2	7	6	F1	1	1474.69051(1)	4.432E-22	0.06	Air	0.0672(1)	1.10(1)	+0.00045(9)	-0.000005(2)
											Self	0.0746(2)	0.46(1)	-0.00318(17)	+0.000005(3)
6	P	5	F1	7	6	F2	2	1474.76836(1)	3.841E-22	0.10	Air	0.0675(1)	1.12(1)	-0.00060(11)	+0.000011(2)
											Self	0.0743(1)	0.49(1)	-0.00029(16)	-0.000001(3)
7	R	7	F2	6	6	F1	1	1608.60542(7)	3.901E-23	0.72	Air	0.0693(6)	1.15(5)		
											Self	0.0692(3)	0.82(2)		
7	R	7	F1	7	6	F2	2	1608.62362(4)	7.302E-23	0.38	Air	0.0689(3)	1.07(3)		
											Self	0.0704(2)	0.61(1)		
7	R	7	F2	7	6	F1	1	1609.86970(4)	6.555E-23	0.17	Air	0.0681(3)	1.07(2)	+0.00331(30)	+0.000011(8)
											Self	0.0677(1)	0.71(1)	+0.00116(19)	0.000000(4)
7	R	7	A2	3	6	A1	1	1610.09139(1)	4.938E-22	0.07	Air	0.0611(0)	1.11(1)	-0.00001(6)	-0.000017(2)
											Self	0.0701(1)	0.46(1)	-0.00204(7)	-0.000011(1)
7	R	7	F2	8	6	F1	1	1610.59595(2)	1.647E-22	0.06	Air	0.0633(1)	1.04(1)	-0.00228(12)	+0.000013(3)
											Self	0.0672(1)	0.64(1)	-0.00389(9)	+0.000008(2)
7	R	7	F1	8	6	F2	2	1610.77793(2)	1.403E-22	0.08	Air	0.0632(1)	1.08(1)	-0.00320(14)	+0.000058(3)
											Self	0.0675(1)	0.60(1)	-0.00523(12)	-0.000002(2)
7	R	7	A1	3	6	A2	1	1610.95104(1)	2.836E-22	0.06	Air	0.0636(1)	1.09(1)	-0.00603(8)	+0.000037(2)
											Self	0.0711(1)	0.52(1)	-0.00562(7)	+0.000021(1)
7	R	7	F1	9	6	F2	2	1614.02300(7)	3.266E-23	0.58	Air	0.0674(8)	0.77(8)	-0.00214(86)	+0.000116(22)
											Self	0.0696(7)	0.48(5)	+0.00039(82)	+0.000070(15)
7	R	7	F1	9	6	F2	1	1614.04497(3)	9.200E-23	0.25	Air	0.0694(4)	0.95(4)	-0.00809(44)	-0.000016(12)
											Self	0.0766(5)	0.37(3)	-0.00637(49)	+0.000024(8)
7	R	7	E	6	6	E	1	1614.07730(3)	7.809E-23	0.20	Air	0.0659(3)	0.97(3)	-0.00835(29)	-0.000004(8)
											Self	0.0717(2)	0.48(2)	-0.00802(28)	+0.000010(5)
7	R	7	F2	9	6	F1	1	1614.27501(14)	1.030E-23	0.62	Air				
											Self	0.0728(4)		+0.00069(46)	
7	P	6	F1	6	7	F2	2	1462.63725(5)	4.527E-23	0.29	Air	0.0676(4)	0.78(4)	-0.00379(43)	-0.000042(12)
											Self	0.0723(3)	0.46(2)	-0.00178(35)	+0.000016(7)
7	P	6	F1	6	7	F2	1	1462.67578(2)	1.252E-22	0.10	Air	0.0680(1)	1.07(2)	-0.00650(18)	+0.000011(5)
											Self	0.0749(1)	0.52(1)	-0.00681(15)	+0.000015(3)
7	P	6	F2	7	7	F1	1	1463.02716(2)	9.779E-23	0.05	Air	0.0706(1)	1.09(1)	-0.00833(16)	+0.000056(5)
											Self	0.0741(1)	0.59(1)	-0.00923(11)	+0.000035(2)
7	P	6	E	5	7	E	1	1463.38101(4)	5.550E-23	0.08	Air	0.0733(2)	0.96(2)	-0.00335(27)	+0.000034(7)
											Self	0.0759(2)	0.64(1)	-0.00466(16)	+0.000014(3)
7	P	6	F1	7	7	F2	2	1463.52270(6)	2.964E-23	0.16	Air	0.0669(4)	1.05(4)	-0.00462(43)	+0.000050(12)
											Self	0.0694(2)	0.67(2)	-0.00375(25)	+0.000027(5)
7	P	6	F2	8	7	F1	2	1465.71274(1)	6.165E-22	0.04	Air	0.0633(1)	1.08(1)	-0.00164(6)	-0.000010(1)
											Self	0.0729(1)	0.39(1)	-0.00228(9)	+0.000028(2)

Table 2 (continued)

<i>lml</i>	ΔJ	<i>J'</i>	<i>C'</i>	<i>n'</i>	<i>J''</i>	<i>C''</i>	<i>n''</i>	Position ^a	Intensity ^b	% unc	Broadening gas	Width ^c	Width temp dependence ^d	Shift ^e	Shift temp dependence ^e
7	P	6	E	6	7	E	1	1465.90975(1)	3.042E-22	0.10	Air Self	0.0569(1) 0.0658(3)	1.04(1) 0.34(2)	-0.00084(10) +0.00139(22)	-0.000031(3) +0.000046(5)
7	P	6	F1	8	7	F2	2	1465.95296(1)	4.201E-22	0.08	Air Self	0.0658(1) 0.0777(3)	1.15(1) 0.24(3)	-0.00150(8) +0.00040(29)	
7	P	6	A1	3	7	A2	1	1466.01423(1)	6.464E-22	0.06	Air Self	0.0603(1) 0.0718(2)	1.03(1) 0.33(1)	-0.00062(5) -0.00018(8)	
8	R	8	F1	8	7	F2	2	1620.97601(6)	2.034E-23	0.47	Air Self	0.0618(7) 0.0663(5)	1.12(8) 0.53(4)		
8	R	8	F2	9	7	F1	2	1621.86220(2)	1.359E-22	0.09	Air Self	0.0610(1) 0.0674(1)	1.05(1) 0.55(1)	-0.00207(13) -0.00283(10)	+0.000005(3) -0.000002(2)
8	R	8	E	6	7	E	1	1621.98947(2)	1.291E-22	0.08	Air Self	0.0447(1) 0.0550(1)	0.95(1) 0.41(1)	-0.00367(8) -0.00355(8)	+0.000010(2) +0.000018(2)
8	R	8	F1	9	7	F2	2	1622.21603(2)	1.201E-22	0.12	Air Self	0.0618(1) 0.0683(1)	1.05(2) 0.55(1)	-0.00261(17) -0.00348(14)	+0.000005(5) +0.000017(3)
8	R	8	F1	9	7	F2	1	1622.25432(5)	4.928E-23	0.24	Air Self	0.0629(3) 0.0703(3)	1.04(4) 0.48(2)	-0.01184(37) -0.01057(32)	+0.000092(10) +0.000051(6)
8	R	8	A1	4	7	A2	1	1626.52935(2)	2.047E-22	0.12	Air Self	0.0679(1) 0.0716(2)	1.00(1) 0.55(1)	-0.00702(16) -0.00696(20)	+0.000040(5) +0.000011(4)
8	R	8	F1	10	7	F2	2	1626.56124(8)	3.998E-23	0.58	Air Self	0.0632(7) 0.0773(12)	1.06(7) 0.24(7)	-0.00894(85) -0.00669(133)	+0.000018(22) -0.000008(23)
8	R	8	F1	10	7	F2	1	1626.59912(4)	7.149E-23	0.28	Air Self	0.0636(4) 0.0699(5)	0.97(3) 0.48(3)	-0.00524(44) -0.00842(60)	+0.000053(11) +0.000003(11)
8	R	8	F2	10	7	F1	1	1626.63297(3)	1.003E-22	0.19	Air Self	0.0649(2) 0.0692(2)	0.95(2) 0.58(2)	-0.00785(25) -0.00838(30)	+0.000054(7) +0.000024(6)
8	P	7	E	5	8	E	1	1453.01036(3)	8.227E-23	0.12	Air Self	0.0662(2) 0.0692(2)	1.26(2) 0.53(1)	-0.00627(25) -0.00837(18)	+0.000029(7) +0.000020(4)
8	p	7	F2	7	8	F1	1	1453.07752(2)	1.039E-22	0.11	Air Self	0.0643(2) 0.0706(1)	1.13(2) 0.57(1)	-0.00752(19) -0.00689(14)	+0.000025(5) +0.000040(3)
8	P	7	A2	3	8	A1	1	1453.30619(2)	1.539E-22	0.06	Air Self	0.0694(1) 0.0734(1)	1.11(1) 0.59(1)	-0.00720(16) -0.00876(11)	+0.000019(4) +0.000023(2)
8	p	7	F2	8	8	F1	2	1453.73260(3)	7.276E-23	0.10	Air Self	0.0624(2) 0.0674(1)	1.04(2) 0.60(1)	-0.00796(21) -0.00751(13)	+0.000016(6) +0.000025(3)
8	P	7	F1	8	8	F2	1	1453.92734(6)	2.636E-23	0.33	Air Self	0.0666(3) 0.0675(3)	0.65(2)	-0.00143(29)	+0.000009(6)
9	R	9	F2	8	8	F1	2	1630.40222(6)	4.093E-23	0.06	Air Self	0.0671(8) 0.0677(6)	1.02(9) 0.70(5)	+0.00452(79) +0.00339(33)	+0.000025(24)
9	R	9	F1	8	8	F2	1	1630.41467(5)	4.928E-23	0.05	Air Self	0.0600(6) 0.0669(5)	0.91(7) 0.56(4)	-0.00003(59) -0.00094(36)	+0.000003(17) -0.000017(6)
9	R	9	E	6	8	E	2	1632.10918(4)	7.263E-23	0.09	Air Self	0.0739(5) 0.0630(6)	1.13(5) 0.91(5)		+0.00484(21) +0.000027(5)
9	R	9	F1	9	8	F2	2	1632.11704(4)	6.231E-23	0.09	Air Self	0.0561(4) 0.0762(9)	0.87(5) 0.27(6)		
9	R	9	F1	10	8	F2	2	1633.15072(2)	1.635E-22	0.09	Air Self	0.0605(1) 0.0663(1)	0.99(1) 0.58(1)	-0.00342(10) -0.00347(11)	+0.000021(2) +0.000019(2)
9	R	9	E	7	8	E	2	1633.49223(3)	6.537E-23	0.11	Air Self	0.0489(1) 0.0558(1)	0.95(2) 0.60(1)	-0.00124(16) -0.00291(13)	+0.000003(4) -0.000009(3)
9	R	9	F2	10	8	F1	2	1633.56625(2)	1.380E-22	0.07	Air Self	0.0601(2) 0.0664(1)	1.07(2) 0.57(1)	-0.00664(17) -0.00618(13)	+0.000025(5) +0.000037(2)

Table 2 (continued)

lml	ΔJ	J'	C'	n'	J''	C''	n''	Position ^a	Intensity ^b	% unc	Broadening gas	Width ^c	Width temp dependence ^d	Shift ^e	Shift temp dependence ^e
10	P	9	E	6	10	E	1	1433.87905(15)	5.014E-23	2.19	Air Self	0.0606(10) 0.0675(8)		+0.00441(146) -0.00800(232)	
10	P	9	F1	9	10	F2	1	1433.89002(10)	8.386E-23	1.31	Air Self	0.0675(8) 0.0704(6)		-0.01128(123) -0.00720(200)	
10	P	9	A1	3	10	A2	1	1433.91214(3)	1.479E-22	0.26	Air Self	0.0573(3) 0.0677(4)	1.01(3) 0.39(3)	-0.00818(24) -0.00872(43)	+0.000005(6) +0.000047(7)
10	P	9	F2	9	10	F1	2	1434.63100(11)	2.846E-23	0.39	Air Self	0.0678(7) 0.0694(8)	0.96(7) 0.72(5)	-0.00353(75) -0.00406(84)	-0.000051(20) +0.000011(15)
10	P	9	F2	9	10	F1	1	1434.70628(6)	5.093E-23	0.24	Air Self	0.0613(4) 0.0647(5)	0.92(4) 0.68(3)	-0.00596(39) -0.00738(47)	+0.000045(10) +0.000012(8)
10	P	9	F1	10	10	F2	2	1434.80684(7)	4.283E-23	0.23	Air Self	0.0661(4) 0.0680(5)	0.95(5) 0.73(3)	-0.00858(47) -0.00778(55)	+0.000053(13) +0.000044(10)
11	Q	11	F1	14	11	F2	3	1550.60963(6)	4.518E-23	0.33	Air Self	0.0603(3) 0.0638(3)	0.84(4) 0.68(2)	+0.00419(29) -0.00020(35)	-0.000024(9) -0.000032(7)
11	Q	11	F1	13	11	F2	2	1550.68880(10)	2.700E-23	0.63	Air Self	0.0505(5) 0.0589(6)	0.90(9) 0.56(5)	-0.00188(55) -0.00584(66)	+0.000091(18) -0.000010(13)
11	Q	11	E	9	11	E	1	1550.71969(4)	7.350E-23	0.33	Air Self	0.0593(3) 0.0621(3)	0.89(4) 0.66(3)	-0.00292(29) -0.00543(36)	+0.000015(10) 0.000000(7)
11	Q	11	F1	14	11	F2	2	1550.75086(7)	4.095E-23	0.46	Air Self	0.0523(4) 0.0571(4)	0.95(6) 0.68(4)	-0.00544(37) -0.00474(43)	+0.000001(12) +0.000039(9)
11	Q	11	F1	13	11	F2	1	1550.85765(1)	2.295E-22	0.10	Air Self	0.0436(1) 0.0553(2)	0.87(1) 0.50(1)	-0.00375(7) -0.00495(15)	+0.000015(2) +0.000012(3)
11	Q	11	F2	13	11	F1	1	1550.91759(1)	2.512E-22	0.10	Air Self	0.0445(1) 0.0560(2)	0.92(1) 0.45(1)	-0.00602(8) -0.00592(16)	+0.000032(3) +0.000030(3)
11	Q	11	A1	5	11	A2	1	1551.11911(2)	1.416E-22	0.12	Air Self	0.0673(1) 0.0666(1)	1.08(1) 0.64(1)	-0.00589(12) -0.00693(14)	+0.000014(4) +0.000045(3)
12	Q	12	F2	14	12	F1	2	1553.54679(15)	1.450E-23	0.97	Air Self	0.0520(6) 0.0579(6)			
12	Q	12	F1	14	12	F2	3	1553.59291(13)	1.785E-23	0.84	Air Self	0.0620(7) 0.0656(7)	0.48(5) 0.55(5)	-0.00424(49)	
12	Q	12	A1	5	12	A2	1	1553.68345(6)	7.737E-23	0.57	Air Self	0.0654(4) 0.0660(5)	1.13(4) 0.79(4)	+0.00136(45) +0.00124(65)	-0.000021(13) +0.000013(12)
12	Q	12	F1	14	12	F2	2	1553.70020(35)	1.092E-23	3.57	Air Self	0.0498(18) 0.0578(31)		-0.00535(243) -0.01370(356)	
12	Q	12	E	10	12	E	1	1553.76322(3)	1.247E-22	0.32	Air Self	0.0403(2) 0.0502(4)	1.06(3) 0.49(3)	-0.00386(20) -0.00824(37)	+0.000010(6) +0.000012(7)
12	Q	12	F2	14	12	F1	1	1553.78283(2)	1.648E-22	0.21	Air Self	0.0390(1) 0.0516(3)	0.91(2) 0.47(3)	-0.00408(13) -0.00619(27)	+0.000040(4) +0.000005(5)
12	Q	12	F1	14	12	F2	1	1553.84120(8)	4.430E-23	0.54	Air Self	0.0457(4) 0.0554(6)	1.25(6) 0.63(6)	-0.00167(42) -0.00281(71)	+0.000059(13) +0.000053(13)
12	Q	12	A2	5	12	A1	1	1553.87492(1)	3.130E-22	0.11	Air Self	0.0414(1) 0.0535(2)	0.93(1) 0.49(1)	-0.00621(7) -0.00612(14)	+0.000034(2) +0.000027(3)
12	Q	12	F2	15	12	F1	1	1553.99385(12)	1.732E-23	0.64	Air Self	0.0452(5) 0.0531(4)	1.33(9) 0.69(4)	-0.00921(53) -0.00734(45)	+0.000016(18) +0.000026(10)
12	P	11	A2	4	12	A1	1	1414.96672(4)	6.938E-23	0.16	Air Self	0.0557(2) 0.0579(2)	0.84(2) 0.83(1)	-0.00744(27) -0.00832(25)	+0.000037(7) +0.000025(5)
12	P	11	F2	10	12	F1	1	1415.02592(6)	4.227E-23	0.33	Air Self	0.0555(4) 0.0563(3)	0.78(5) 0.92(3)	-0.00569(42) -0.00879(43)	+0.000009(12) -0.000003(9)

12	P	11	E	7	12	E	1	1415.05954(9)	2.870E-23	0.49	Air Self	0.0558(5) 0.0567(4)	0.89(6) 1.00(4)	-0.00662(60) -0.00511(57)	-0.000005(18) +0.000055(12)
13	P	12	E	8	13	E	1	1406.65734(23)	1.216E-23	0.68	Air Self	0.0630(14) 0.0643(10)	0.83(18) 0.66(9)	-0.00254(149) -0.00976(111)	+0.000111(48) +0.000006(24)
13	P	12	F2	12	13	F1	2	1406.73345(17)	1.653E-23	0.49	Air Self	0.0611(10) 0.0619(7)	1.23(14) 0.87(6)	-0.00410(107) -0.00701(81)	+0.000131(35) +0.000020(18)
13	P	12	A2	4	13	A1	1	1407.20173(7)	3.936E-23	0.18	Air Self	0.0527(3) 0.0585(3)	0.98(5) 0.71(3)	-0.00391(39) -0.00638(32)	-0.000027(12) -0.000035(7)
14	P	13	F1	15	14	F2	2	1411.03220(6)	4.490E-23	0.25	Air Self	0.0373(2) 0.0476(2)	1.10(6) 0.71(3)	-0.00091(27) -0.00324(28)	+0.000020(9) +0.000008(6)
14	P	13	F2	15	14	F1	1	1411.07364(6)	4.636E-23	0.30	Air Self	0.0439(3) 0.0521(3)	0.95(6) 0.67(3)	+0.00068(31) -0.00273(32)	+0.000059(10) +0.000001(7)
14	P	13	A2	6	14	A1	1	1411.14901(2)	1.269E-22	0.07	Air Self	0.0408(1) 0.0517(1)	0.96(2) 0.60(1)	-0.00155(11) -0.00338(12)	+0.000016(3) +0.000016(3)
14	P	13	F2	16	14	F1	2	1411.29815(4)	7.946E-23	0.12	Air Self	0.0503(2) 0.0556(2)	0.91(3) 0.72(2)	+0.00092(20) -0.00054(19)	-0.000020(6) +0.000007(4)
14	P	13	E	10	14	E	2	1411.36847(5)	5.746E-23	0.17	Air Self	0.0412(2) 0.0505(2)	0.71(4) 0.64(2)	-0.00179(23) -0.00404(23)	+0.000002(7) +0.000011(5)
14	P	13	F1	16	14	F2	3	1411.44327(3)	9.762E-23	0.09	Air Self	0.0511(1) 0.0562(2)	0.97(3) 0.68(2)	-0.00483(17) -0.00594(16)	+0.000040(5) +0.000023(4)
14	P	13	F2	17	14	F1	3	1412.15272(4)	9.881E-23	0.33	Air Self	0.0320(2) 0.0399(2)	0.80(5) 0.53(3)	+0.00699(21) +0.00001(27)	-0.000035(6) -0.000061(6)
14	P	13	E	11	14	E	3	1412.16923(4)	9.727E-23	0.36	Air Self	0.0193(2) 0.0265(2)	0.77(6) 0.55(5)	-0.00139(17) -0.00441(26)	+0.000008(5) +0.000013(5)
14	P	13	F1	17	14	F2	4	1412.18781(3)	1.065E-22	0.27	Air Self	0.0343(2) 0.0426(2)	0.84(4) 0.60(3)	-0.01249(21) -0.01137(26)	+0.000076(6) +0.000086(5)
15	Q	15	F1	19	15	F2	2	1563.25237(5)	3.956E-23	0.18	Air Self	0.0297(1) 0.0428(2)	0.88(5) 0.47(2)	-0.00454(17) -0.00554(18)	+0.000036(7) +0.000014(4)
15	Q	15	F2	17	15	F1	1	1563.31653(5)	3.975E-23	0.17	Air Self	0.0310(1) 0.0431(1)	0.79(5) 0.54(2)	-0.00459(17) -0.00588(19)	+0.000063(7) +0.000020(5)
15	Q	15	E	12	15	E	1	1563.74815(14)	1.363E-23	0.40	Air Self	0.0423(5) 0.0505(5)	1.17(14) 0.69(6)	-0.00285(56) -0.00316(53)	-0.000049(26) +0.000016(13)
15	Q	15	F1	18	15	F2	2	1563.85786(11)	1.805E-23	0.31	Air Self	0.0416(4) 0.0509(4)	1.05(11) 0.55(5)	-0.00394(43) -0.00493(40)	-0.000042(20) +0.000020(10)
15	Q	15	A1	6	15	A2	1	1564.30306(7)	3.118E-23	0.24	Air Self	0.0462(2) 0.0537(2)	1.05(7) 0.49(3)	-0.00326(29) -0.00525(27)	+0.000101(13) -0.000018(7)
15	P	14	A2	6	15	A1	1	1405.79540(2)	1.103E-22	0.30	Air Self	0.0506(8) 0.0557(18)	0.92(5)	-0.00241(51)	+0.000016(11)
15	P	14	F2	18	15	F1	4	1405.81859(3)	6.308E-23	0.56	Air Self	0.0371(11) 0.0169(26)			
15	P	14	F1	18	15	F2	4	1405.84213(3)	6.456E-23	0.55	Air Self	0.0318(10) 0.0324(25)			
15	P	14	A1	7	15	A2	2	1405.86549(2)	1.152E-22	0.30	Air self	0.0539(7) 0.0546(17)	1.11(4)	-0.00676(52)	+0.000165(11)
16	Q	16	E	12	16	E	1	1566.62363(13)	1.420E-23	0.77	Air Self	0.0281(4) 0.0373(4)	1.36(17) 0.86(8)	-0.00677(46) -0.00439(42)	+0.000049(21) +0.000084(10)
16	Q	16	F2	18	16	F1	1	1566.65064(9)	2.036E-23	0.54	Air Self	0.0274(3) 0.0391(2)	0.59(12) 0.0391(2)	-0.00571(33) -0.00473(35)	+0.000021(14) +0.000047(8)
16	Q	16	A2	7	16	A1	1	1566.71306(5)	3.439E-23	0.20	Air Self	0.0292(1) 0.0393(2)	0.97(7) 0.62(3)	-0.00572(20) -0.00678(18)	+0.000047(8) +0.000028(5)
16	Q	16	F2	19	16	F1	2	1567.39507(18)	1.081E-23	0.47	Air Self	0.0391(5) 0.0454(3)		-0.00469(61) -0.00425(35)	

Table 2 (continued)

lml	ΔJ	J'	C	n'	J''	C''	n''	Position ^a	Intensity ^b	% unc	Broadening gas	Width ^c	Width temp dependence ^d	Shift ^c	Shift temp dependence ^e
16	Q	16	F1	18	16	F2	1	1567.62860(21)	1.005E-23	0.65	Air	0.0412(6)		-0.00486(72)	
											Self	0.0496(3)		-0.00524(44)	
16	Q	16	A1	7	16	A2	1	1567.73327(21)	1.109E-23	0.59	Air	0.0519(7)		+0.00130(80)	
											Self	0.0543(4)		-0.00307(45)	
16	P	15	A2	6	16	A1	2	1398.50993(8)	5.261E-23	0.40	Air	0.0511(7)	0.71(11)	-0.00273(80)	+0.000072(23)
											Self	0.0558(3)		-0.00729(35)	
16	P	15	F2	19	16	F1	4	1399.79524(7)	3.519E-23	0.68	Air	0.0480(1)	1.11(14)	-0.00024(17)	-0.000042(38)
											Self	0.0560(20)	0.40(17)	-0.00583(217)	+0.000037(41)
16	P	15	E	13	16	E	3	1399.82192(13)	2.373E-23	1.43	Air	0.0173(10)	0.87(35)	-0.00449(84)	+0.000031(20)
											Self	0.0258(16)	0.27(31)	-0.00812(136)	+0.000026(26)
16	P	15	F1	20	16	F2	4	1399.84755(12)	3.670E-23	0.87	Air	0.0518(14)	0.57(14)	-0.00792(189)	+0.000123(40)
											Self	0.0501(16)	1.42(15)	-0.00963(293)	-0.000056(54)

Values in parentheses are statistical uncertainties in units of the last digit quoted; (0) means that the uncertainty is less than half a unit.

^a Positions are given in cm^{-1} .

^b Intensities are in units of $\text{cm}^{-1}/(\text{molecule cm}^{-2})$ at 296 K. Percent statistical uncertainties are given in the adjoining column.

^c Half width and pressure-induced shift coefficients are in units of $\text{cm}^{-1} \text{atm}^{-1}$ at 296 K.

^d Half width temperature dependence exponents are unitless.

^e Temperature dependences of shift coefficients are in units of $\text{cm}^{-1} \text{atm}^{-1} \text{K}^{-1}$.

study, the mean and standard deviation of the differences in line positions between the present results and the HITRAN04 [29] values are $3.9 \times 10^{-5} \text{ cm}^{-1}$ and $2.7 \times 10^{-4} \text{ cm}^{-1}$, respectively, and the mean and standard deviation of ratios of line intensities (present work divided by HITRAN value) are 0.99 and 0.04 for HITRAN04 [29]. The agreement of positions and intensities with our measurements is the same or slightly better for both subsequent HITRAN editions.

3.1. Half width and pressure-induced shift coefficients

The air- and self-broadened half width and shift coefficients determined from the multispectrum fits in the ν_2 band are listed in Table 2, and in Fig. 5 they are plotted as functions of m using different symbols for A-, E- and F-species transitions. ($m = -J'', J''$, and $J'' + 1$ for P-, Q- and R-branch transitions, respectively.) The uncertainties correspond to one sigma standard deviations in measured quantities. Where error bars are not visible the uncertainties are smaller than the size of the symbols used. The measured half width coefficients (panels (a) and (b)) in both air- and self broadening range between ~ 0.02 and $0.08 \text{ cm}^{-1} \text{atm}^{-1}$ at 296 K. Both sets of half width coefficients decrease with increasing $|m|$. This is similar to what has been observed in the ν_4 bands of $^{12}\text{CH}_4$ and $^{13}\text{CH}_4$ [1–3]. Also similar to the ν_4 results, the ratio of self- to air-broadened half width in the ν_2 band varies from line to line, with the majority of these ratios having values between 1.0 and 1.5, and the higher ratios occurring with larger $|m|$ values.

Most of the shift coefficients (panels (c) and (d)) are negative, although a few positive shift coefficients were also obtained for both air and self broadening. The shift coefficients roughly range between $+0.007 \text{ cm}^{-1} \text{atm}^{-1}$ and $-0.020 \text{ cm}^{-1} \text{atm}^{-1}$ at 296 K for air broadening and from $+0.005 \text{ cm}^{-1} \text{atm}^{-1}$ to $-0.023 \text{ cm}^{-1} \text{atm}^{-1}$ at 296 K for self broadening. Similar ranges of shift values were observed in the ν_4 bands of $^{12}\text{CH}_4$ and $^{13}\text{CH}_4$ [1–3], although there is considerably more scatter among the measurements in the weaker ν_2 band. In both the ν_2 and ν_4 bands of $^{12}\text{CH}_4$ the measured values of the pressure-induced shifts show no obvious dependence on either the rotational quantum number index m or the symmetry of the transition. The mean values of the ν_2 pressure-induced shifts are $-0.0037 \text{ cm}^{-1} \text{atm}^{-1}$ at 296 K for air-shifts and $-0.0046 \text{ cm}^{-1} \text{atm}^{-1}$ at 296 K for self-shifts, while for the ν_4 band the mean values were $-0.0033 \text{ cm}^{-1} \text{atm}^{-1}$ at 296 K for air-shifts [1] and $-0.0042 \text{ cm}^{-1} \text{atm}^{-1}$ at 296 K for self-shifts [2]. Thus, on average, the pressure-induced shifts in the ν_2 and ν_4 bands are very similar.

3.2. Temperature dependences of half width and pressure-induced shift coefficients

Because the ν_2 band lines are weaker than the ν_4 band lines, a smaller number of observed spectra were included in the retrievals (29 for ν_2 (see Table 1); 60 for ν_4 [1,2]), although the temperature range was nearly the same for both bands. Therefore, the results for the temperature dependences of the ν_2 air- and self-broadened half width and shift coefficients should be considered less accurate

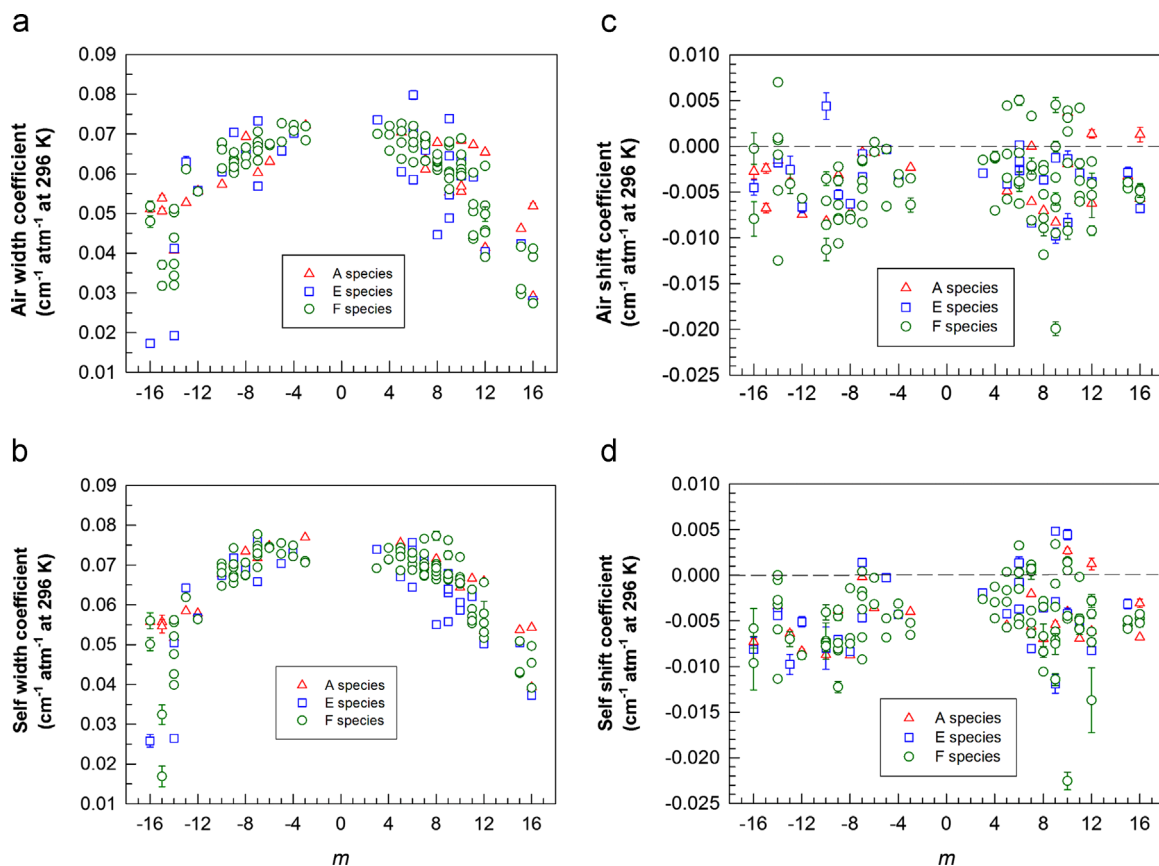


Fig. 5. Measured $^{12}\text{CH}_4$ ν_2 half width and shift coefficients in $\text{cm}^{-1} \text{atm}^{-1}$ at 296 K plotted vs. m ($m = -J'', J''$ and $J'' + 1$ for P-, Q- and R-branch transitions, respectively). Air-broadened widths and shifts are shown in the upper panels (a) and (c), and the self-broadened widths and shifts are given in the lower panels (b) and (d). In each plot triangle, square, and circle symbols are used to indicate values for the A-, E- and F-species transitions, respectively. Where error bars are not visible the statistical uncertainty in the measured value is smaller than the size of the symbol used.

than the corresponding ν_4 values. The more limited accuracy may be seen in the statistical uncertainties associated with the measured values reported in Table 2, which are represented by the error bars in Fig. 6.

As seen in Table 2, we were able to determine through multispectrum fits the temperature dependence exponents of the air- and self-broadened half width coefficients, n_1 and n_2 defined in Eq. (1), for most of the ν_2 transitions measured. Fig. 6(a) and (b) are plots of the measured air- and self-broadened half width temperature dependence exponents n_1 and n_2 vs. m . As with the air- and self-broadened half width coefficients (Fig. 5(a) and (b)), the temperature dependence exponents are also transition dependent, but show different distributions with m . The values of n_1 range between 0.4 and 1.4, and the values of n_2 vary from 0.2 to 1.0, indicating that the temperature dependence exponents for self-broadening are smaller than for air broadening. These ranges of n_1 and n_2 are consistent with those determined from multispectrum fits in the ν_4 band [1,2], although the ν_4 results showed a wider range, including some negative values for n_2 .

The measured temperature dependence coefficients δ' for air- and self-shifts from this study, defined in Eq. (3), are plotted vs. m in Fig. 6(c) and (d). Both positive and negative values are obtained for $\delta'(\text{air})$ and $\delta'(\text{self})$. The majority of the temperature dependence coefficients

for both air- and self-shifts are positive with values between zero and $+0.0001 \text{cm}^{-1} \text{atm}^{-1} \text{K}^{-1}$. Since the values of the air- and self-shift coefficients are much smaller than the corresponding half width coefficients, values of $\delta'(\text{air})$ and $\delta'(\text{self})$ are very small and highly uncertain and should be judged as only indicative of the upper limits to $\delta'(\text{air})$ and $\delta'(\text{self})$. Since $\delta^0(\text{air})$ and $\delta^0(\text{self})$ are nearly of equal magnitude, it is not surprising that $\delta'(\text{air})$ and $\delta'(\text{self})$ are also very similar. These results for ν_2 are very similar to those obtained from multispectrum fits in the ν_4 band [1,2]. Our results for $\delta'(\text{air})$ and $\delta'(\text{self})$ in the ν_2 band of CH_4 are the first ever reported.

3.3. Off-diagonal relaxation matrix element coefficients

As stated earlier, a Voigt line shape including speed dependence and line mixing via full relaxation matrix formulation was used to fit the data. The optical densities (pressure-path length products) in the spectral data set available for our analysis of the ν_2 band (see Table 1) were not large enough to easily distinguish these effects. As explained in Section 2, speed dependence parameters could not be determined, and it was not necessary to include line mixing to fit most of the J manifolds. However, it was possible to measure the off-diagonal relaxation

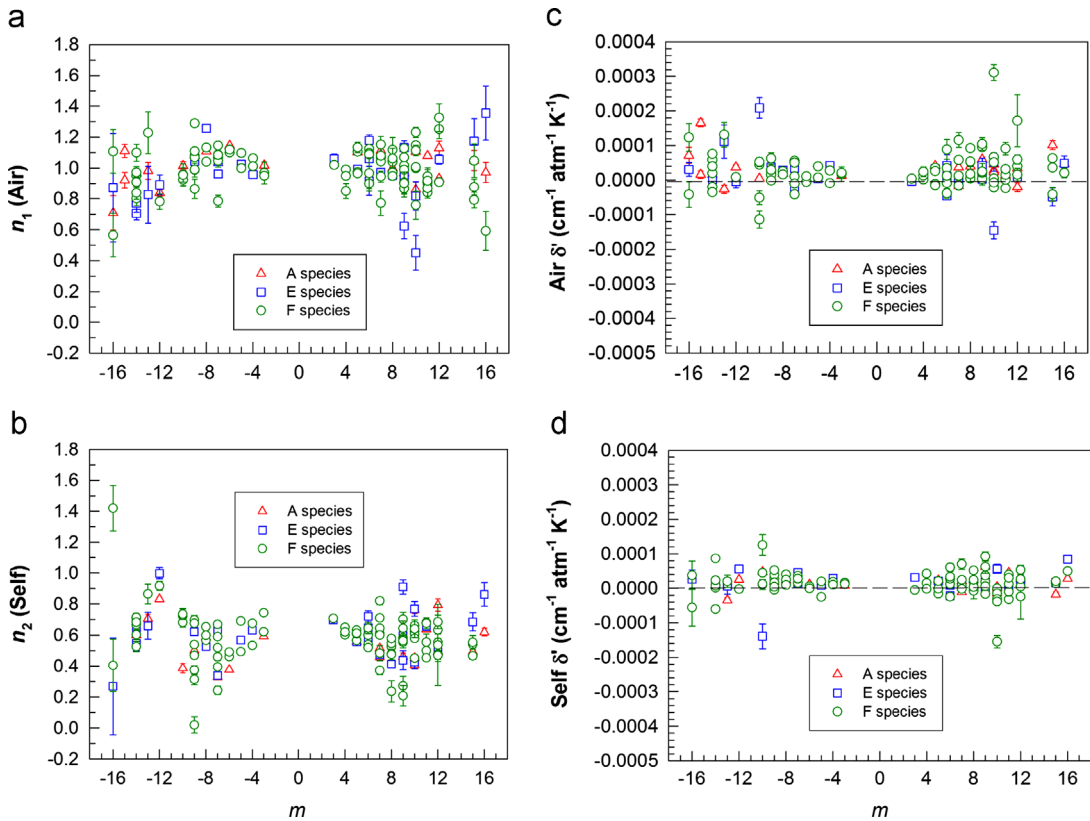


Fig. 6. Temperature dependences for $^{12}\text{CH}_4$ ν_2 half width and shift coefficients determined from the multispectrum fits. Air- (a) and self-broadened (b) half width temperature exponents (Eq. (1)) are unitless, and air (c) and self-broadened (d) shift temperature coefficients (Eq. (3)) are in $\text{cm}^{-1} \text{atm}^{-1} \text{K}^{-1}$. The meanings of the symbols and error bars correspond to those in Fig. 5.

matrix element (ORME) coefficients for both air- and self broadening for 10 pairs of ν_2 transitions. As was the case for the ν_4 bands of $^{12}\text{CH}_4$ and $^{13}\text{CH}_4$ [1–3], the limited temperature range of the set of laboratory spectra made it impossible to uniquely determine the temperature dependence exponents of the ORME coefficients, and these were held fixed to the value 1.0. The measured ORME coefficients are listed in Table 3 for these pairs of ν_2 transitions; five in the P-branch and five in the R-branch J manifolds. Except for two pairs of A-species transitions, all the rest of the mixing coefficients were determined for F-species transitions. The results given in Table 3 suggest that the ORME coefficients for air and self mixing in the ν_2 band are very similar; this has also been noted for ν_4 [1,2]. For comparison, the ORME coefficients for self and air mixing measured for corresponding pairs of transitions in the ν_4 [1,2] and $\nu_2 + \nu_3$ [16] bands are also shown in Table 3. Considering the measurement uncertainties of the ORME coefficients in the three bands, the agreement is good in the majority of the cases, with the larger ORME values usually observed in the higher J manifolds.

For the convenience of the reader who may want to compare the ORME coefficients in Table 3 with Rosenkranz [37] mixing parameters reported for other methane bands (e.g., [11,24]), the separations between the lines of the pairs involved in line mixing are listed in the last column of the table. However, there appears to be no correlation between the line separations and the line mixing coefficients.

3.4. Comparison with other measurements and databases

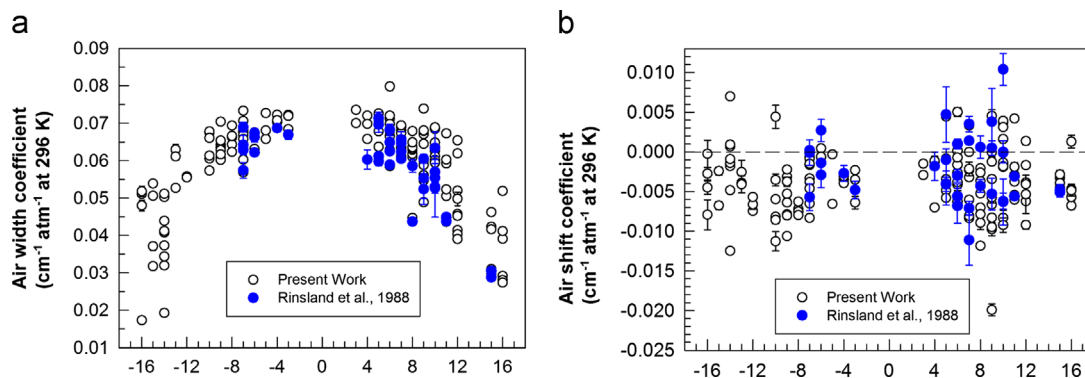
In Fig. 7 the measured air-broadening and pressure-induced shift coefficients from the present work are plotted vs. m again along with the 47 previous measurements of the same parameters reported by Rinsland et al. [18]. Since the ν_2 results in Ref. [18] were based on the five room-temperature spectra listed in Table 1 of this paper, it is not surprising that there is good agreement between the two sets of measurements. However, the width and shift values from the present study have considerably smaller uncertainties and include 154 transitions, more than three times the number reported in Ref. [18].

Since there are no previous measurements of self-broadened half width or shift coefficients in the ν_2 band, or of the temperature dependences of air- or self-broadened widths or shifts in this band, the present results plotted in Figs. 5 and 6 cannot be compared with other experimental results in the same band. Similarities between the ν_2 and ν_4 results have already been noted in the previous three sections of this discussion.

Fig. 8 compares the values resulting from the present study with those in HITRAN04 [29] for ν_2 air- and self-broadened widths, the temperature dependences of the air-broadened widths, and the air pressure-induced shifts. The differences between HITRAN04 and the measured values for ν_2 are similar to those already noted in our previously-reported studies of the ν_4 band [1,2]. That is,

Table 3Measured off-diagonal relaxation matrix element coefficients in the $^{12}\text{CH}_4$ ν_2 band and for corresponding transitions in the ν_4 and $\nu_2 + \nu_3$ bands.

Mixing pair(s)	Assignments	ν (cm^{-1})	Off-diagonal relaxation matrix element coefficients ($\text{cm}^{-1} \text{atm}^{-1}$ at 296 K)		
			Self-broadening	Air-broadening	Line separation (cm^{-1})
P(16) F	15F2 19←16F1 4	1399.7952	0.0283(14)	0.0261(19)	0.0523
	15F1 20←16F2 4	1399.8475	0.0286(2) ^a	0.0300(5) ^a	1.1333
P(9) F	14A2 6←15A1 1	1405.7954		0.0314(10)	0.0701
	14A1 7←15A2 2	1405.8655		0.0302(4) ^a	0.8548
P(7) F	8F1 10←9F2 2	1448.8609	0.0204(17)	0.0231(16)	0.0402
	8F2 10←9F1 3	1448.9011	0.0150(1) ^a	0.0175(0) ^a	0.6834
P(6) F	6F2 8←7F1 2	1465.7127	0.0064(1)	0.0049(1)	0.2403
	6F1 8←7F2 2	1465.9530	0.0087(1) ^a	0.0100(1) ^a	1.4174
R(5) F	5F2 7←6F1 1	1474.6905	0.0079(5) ^b	0.0055(2) ^b	0.3533
	5F1 7←6F2 2	1474.7684	0.0053(1)	0.0038(1)	0.0779
R(6) F	6F2 7←5F1 2	1599.0110	0.0098(1) ^a	0.0101(1) ^a	0.6085
	6F1 7←5F2 1	1599.5594	0.0090(1)	0.0128(3)	0.5484
R(6) F	7F2 8←6F1 1	1610.5960	0.0048(1) ^a	0.0067(0) ^a	0.6351
	7F1 8←6F2 2	1610.7779	0.0105(1)	0.0131(1)	0.1819
R(6) A	7A2 3←6A1 1	1610.0914	0.0093(1) ^a	0.0108(0) ^a	0.1809
	7A1 3←6A2 1	1610.9510	0.0088(4) ^b	0.0079(2) ^b	0.1693
R(7) F	8F2 9←7F1 2	1621.8622	0.0151(1)	0.0154(2)	0.8596
	8F1 9←7F2 2	1622.2160	0.0210(1) ^a	0.0198(0) ^a	1.0325
R(8) F	9F1 10←8F2 2	1633.1507	0.0169(11) ^b	0.0178(5) ^b	0.9873
	9F2 10←8F1 2	1633.5662	0.0126(1)	0.0166(4)	0.3538
			0.0154(1)	0.0188(3)	0.4155
			0.0165(2) ^a	0.0143(1) ^a	0.4685

Assignments and positions (columns 2 and 3) are listed only for the ν_2 transitions.^a ν_4 band [1,2].^b $\nu_2 + \nu_3$ band [16].**Fig. 7.** Measured $^{12}\text{CH}_4$ ν_2 air-broadened half width (a) and shift (b) coefficients (open symbols) compared to the previous measurements of Rinsland et al. [18] (solid symbols).

the observed air-widths and shifts have a wider range of values than HITRAN04, the air-width temperature exponents are nearly all larger than the HITRAN04 values, and most of the measured self-broadened widths are smaller than the HITRAN04 values. As was the case for ν_4 , no comparisons with HITRAN08 [35], or HITRAN 2012 [36] need to be done because the ν_2 measured broadening and shifting parameters from the present study were included

in the 2008 edition of the database [35] and carried forward to the 2012 edition [9,36].

We note that, although the broadening and shift parameters and temperature dependences from the present study and Refs. [1–3] were determined through multi-spectrum fits that included line mixing, HITRAN [36] and other widely-used molecular databases currently do not list mixing parameters for methane. Tran et al. [38] have

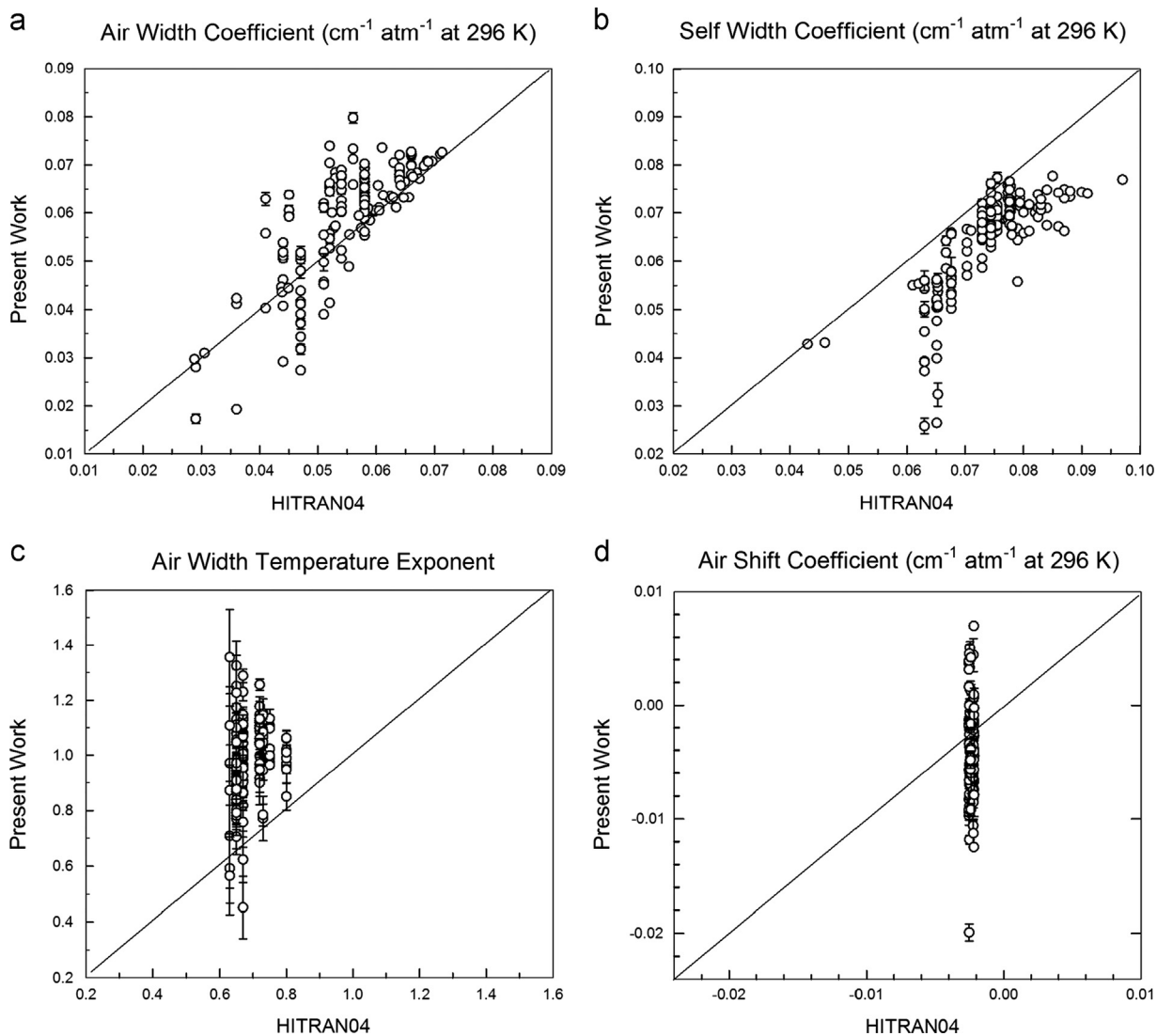


Fig. 8. Comparison of measured $^{12}\text{CH}_4$ ν_2 air- (a) and self-broadened (b) half width coefficients, air-width temperature exponents (c) and air-shift coefficients (d) from the present work to the values given for the same transitions in HITRAN04 [29]. The diagonal line in each panel corresponds to a one-to-one ratio.

examined for the CH_4 $2\nu_3$ band how small residuals in atmospheric retrievals may arise from the use of Voigt profiles without line mixing in forward-model calculations with width and shift parameters that were determined from laboratory spectra using line mixing. One possible solution they discuss is the development of effective (ad hoc) width and shift parameters to be used with the Voigt line shape model. Additional study and discussion is needed to develop solutions that will meet the needs of the community of spectroscopic database users.

3.5. Summary and conclusion

A multispectrum nonlinear least squares fitting procedure was used to analyze 29 spectra in the 1400–1645 cm^{-1} region to obtain spectroscopic parameters for 154 transitions in the ν_2 $^{12}\text{CH}_4$ band. Lorentz air- and self-

broadened half width and air- and self-induced pressure shift coefficients, as well as their temperature dependences between 226 and 297 K, were determined for at least 127 of these transitions. The present study represents the first experimental determination of self-broadened half width and self-induced pressure shift coefficients for the ν_2 CH_4 transitions, as well as the first determinations of temperature dependences of air- and self-broadened half width and pressure-induced shift coefficients in this band. The present analysis also provided accurate values for line positions and absolute line intensities which compare well with the values provided in the three most recent editions of the HITRAN database. Line mixing parameters for both air- and self broadening were determined for the first time in this band (for 10 pairs of transitions). The mixing parameters (off-diagonal relaxation matrix element coefficients) experimentally determined for the ν_2 $^{12}\text{CH}_4$ band are in

reasonable agreement with those determined for transitions with similar rotational quanta in the ν_4 bands of $^{12}\text{CH}_4$ and $^{13}\text{CH}_4$, as well as in the $\nu_2 + \nu_3$ band of $^{12}\text{CH}_4$. The present results should be useful to develop more accurate theoretical models for methane line shapes in the ν_2 and other bands, leading to better understanding of collisional effects in methane and similar tetrahedral molecules.

Acknowledgments

The authors would like to thank Claude Plymate and Mike Dulick of the National Solar Observatory (NSO) for their assistance with the FTS laboratory measurements on Kitt Peak. Research at the College of William and Mary is supported under contracts and cooperative agreements with the National Aeronautics and Space Administration. A. Predoi-Cross acknowledges the financial support received from the National Sciences and Engineering Research Council of Canada (NSERC). We thank NASA's Upper Atmosphere Research Program for their past support of the McMath–Pierce FTS laboratory facility.

Appendix A. Supplementary Information

Supplementary data associated with this article can be found in the online version at <http://dx.doi.org/10.1016/j.jqsrt.2013.08.004>.

References

- [1] Smith MAH, Benner DC, Predoi-Cross A, Malathy Devi V. Multi-spectrum analysis of $^{12}\text{CH}_4$ in the ν_4 spectral region: I. Air-broadened half widths, pressure-induced shifts, temperature dependences and line mixing. *J Quant Spectrosc Radiat Transfer* 2009;110:639–53.
- [2] Smith MAH, Benner DC, Predoi-Cross A, Malathy Devi V. Multi-spectrum analysis of $^{12}\text{CH}_4$ in the ν_4 spectral region: II. Self-broadened half widths, pressure-induced shifts, temperature dependences and line mixing. *J Quant Spectrosc Radiat Transfer* 2010;111:1152–66.
- [3] Smith MAH, Benner DC, Predoi-Cross A, Malathy Devi V. A multi-spectrum analysis of the ν_4 band of $^{13}\text{CH}_4$: widths, shifts, and line mixing coefficients. *J Quant Spectrosc Radiat Transfer* 2011;112:952–68.
- [4] Predoi-Cross A, Brown LR, Malathy Devi V, Brawley-Tremblay M, Benner DC. Multispectrum analysis of $^{12}\text{CH}_4$ from 4100 to 4635 cm^{-1} : I. Self-broadening coefficients (widths and shifts). *J Mol Spectrosc* 2005;232:231–46.
- [5] Predoi-Cross A, Brawley-Tremblay M, Brown LR, Malathy Devi V, Benner DC. Multispectrum analysis of $^{12}\text{CH}_4$ from 4100 to 4635 cm^{-1} : II. Air-broadening coefficients (widths and shifts). *J Mol Spectrosc* 2006;236:201–15.
- [6] Pine AS, Gabard T. Speed-dependent broadening and line mixing in CH_4 perturbed by Ar and N_2 from multispectrum fits. *J Quant Spectrosc Radiat Transfer* 2000;66:69–92.
- [7] Brown LR, Benner DC, Champion JP, Malathy Devi V, Fejard L, Gamache RR, et al. Methane line parameters in HITRAN. *J Quant Spectrosc Radiat Transfer* 2003;82:219–38.
- [8] Antony BK, Niles DL, Wroblewski SB, Humphrey CM, Gabard T, Gamache RR. N_2 -, O_2 - and air-broadened half-widths and line shifts for transitions in the ν_3 band of methane in the 2276- to 3200- cm^{-1} spectral region. *J Mol Spectrosc* 2008;251:268–81.
- [9] Brown LR, Sung K, Benner DC, Devi VM, Boudon V, Gabard T, et al. Methane line parameters in the HITRAN 2012 database. *J Quant Spectrosc Radiat Transfer* <http://dx.doi.org/10.1016/j.jqsrt.2013.06.020>, in press.
- [10] Benner DC, Rinsland CP, Malathy Devi V, Smith MAH, Atkins D. A multispectrum nonlinear least squares fitting technique. *J Quant Spectrosc Radiat Transfer* 1995;53:705–21.
- [11] Mondelain D, Payan S, Deng W, Camy-Peyret C, Hurtmans D, Mantz AW. Measurement of the temperature dependence of line mixing and pressure broadening parameters between 296 and 90 K in the ν_3 band of $^{12}\text{CH}_4$ and their influence on atmospheric methane retrievals. *J Mol Spectrosc* 2007;244:130–7.
- [12] Mondelain D, Camy-Peyret C, Deng W, Payan S, Mantz AW. Study of molecular line parameters down to very low temperature. *Appl Phys B* 2008;90:227–33.
- [13] Tumuhimbise AT, Hurtmans D, Mondelain D, Mantz AW. Nitrogen-pressure shifts in the ν_3 band of methane measured at several temperatures between 300 and 90 K. *J Mol Spectrosc* 2008;252:239–41.
- [14] Malathy Devi V, Benner DC, Brown LR, Miller CE, Toth RA. Line mixing and speed dependence in CO_2 at 6348 cm^{-1} : positions, intensities, and air- and self-broadening derived with constrained multispectrum analysis. *J Mol Spectrosc* 2007;242:90–117.
- [15] Malathy Devi V, Benner DC, Brown LR, Miller CE, Toth RA. Line mixing and speed dependence in CO_2 at 6227.9 cm^{-1} : constrained multispectrum analysis of intensities and line shapes in the 30013–00001 band. *J Mol Spectrosc* 2007;245:52–80.
- [16] Predoi-Cross A, Unni AV, Heung H, Malathy Devi V, Benner DC, Brown LR. Line mixing effects in the $\nu_2 + \nu_3$ band of methane. *J Mol Spectrosc* 2007;246:65–76.
- [17] Malathy Devi V, Fridovich B, Snyder DGS, Jones GD, Das PP. Tunable diode laser measurements of intensities and Lorentz broadening coefficients of lines in the ν_2 band of $^{12}\text{CH}_4$. *J Quant Spectrosc Radiat Transfer* 1983;29:45–7.
- [18] Rinsland CP, Malathy Devi V, Smith MAH, Benner DC. Measurements of air-broadened and nitrogen-broadened Lorentz width coefficients and pressure shift coefficients in the ν_4 and ν_2 bands of $^{12}\text{CH}_4$. *Appl Opt* 1988;27:631–51.
- [19] Gabard T, Grigorovich IM, Grigorovich NM, Tonkov MV. Helium and argon line broadening in the ν_2 band of CH_4 . *J Mol Spectrosc* 2004;225:123–31.
- [20] Pieroni D, Nguyen-Van-Thanh, Brodbeck C, Hartmann J-M, Gabard T, Champion J-P, et al. Experimental and theoretical study of line mixing in methane spectra. IV. Influence of the temperature and of the band. *J Chem Phys* 2000;113:5776–83.
- [21] Tran H, Flaud P-M, Gabard T, Hase F, von Clarmann T, Camy-Peyret C, et al. Model, software, and database for line-mixing effects in the ν_3 and ν_4 bands of CH_4 and tests using laboratory and planetary measurements. I. N_2 (and air) broadenings and the Earth atmosphere. *J Quant Spectrosc Radiat Transfer* 2006;101:284–301.
- [22] Tran H, Flaud P-M, Fouchet T, Gabard T, Hartmann J-M. Model, software, and database for line-mixing effects in the ν_3 and ν_4 bands of CH_4 and tests using laboratory and planetary measurements. II. H_2 (and He) broadenings and the atmospheres of Jupiter and Saturn. *J Quant Spectrosc Radiat Transfer* 2006;101:306–24.
- [23] Pine AS. Self-, N_2 -, O_2 -, H_2 -, Ar, and He broadening in the ν_3 band Q branch of CH_4 . *J Chem Phys* 1992;97:773–85.
- [24] Pine AS. N_2 and Ar broadening and line mixing in the P and R branches of the ν_3 band of CH_4 . *J Quant Spectrosc Radiat Transfer* 1997;57:157–76.
- [25] Pine AS. Line mixing sum rules for the analysis of multiplet spectra. *J Quant Spectrosc Radiat Transfer* 1997;57:145–55.
- [26] Pine AS, Gabard T. Multispectrum fits for line mixing in the ν_3 band Q branch of methane. *J Mol Spectrosc* 2003;217:105–14.
- [27] Smith MAH, Rinsland CP, Malathy Devi V, Benner DC. Temperature dependence of broadening and shifts of methane lines in the ν_4 band. *Spectrochim Acta* 1992;48A:1257–72.
- [28] Toth RA. ν_2 band of H_2^{16}O : line strengths and transition frequencies. *J Opt Soc Am B* 1991;8:2236–55.
- [29] Rothman LS, Jacquemart D, Barbe A, Benner DC, Birk M, Brown LR, et al. The HITRAN 2004 molecular spectroscopic database. *J Quant Spectrosc Radiat Transfer* 2005;96:139–204.
- [30] Levy A, Lacombe N, Chackerian C. Collisional line mixing. In: Narahari Rao K, Weber A, editors. *Spectroscopy of the Earth's atmosphere and interstellar medium*. Boston, MA: Academic Press; 1992. p. 261–337.
- [31] Lepere M, Valentin A, Henry A, Camy-Peyret C, Blanquet G, Populaire J-C, et al. Pressure broadening study at low temperature: application to methane. *Spectrochim Acta* 2002;A 58:2413–9.
- [32] Lepere M, Valentin A, Henry A, Camy-Peyret C, Lengele M, Populaire J-C, et al. Diode laser spectroscopy: temperature dependence of R(0) line in the ν_4 band of CH_4 perturbed by N_2 and O_2 . *J Mol Spectrosc* 2005;233:86–92.
- [33] Lepere M. Self-broadening coefficients in the ν_4 band of CH_4 by diode-laser spectroscopy. *J Mol Spectrosc* 2006;238:193–9.
- [34] Mantz AW, Malathy Devi V, Benner DC, Smith MAH, Predoi-Cross A, Dulick M. A multispectrum analysis of widths and shifts in the

- 2010 to 2260 cm^{-1} region of $^{12}\text{C}^{16}\text{O}$ broadened by helium at temperatures between 80 and 297 K. *J Mol Struct* 2005;742: 99–110.
- [35] Rothman LS, Gordon IE, Barbe A, Benner DC, Bernath PF, Birk M, et al. The HITRAN 2008 molecular spectroscopic database. *J Quant Spectrosc Radiat Transfer* 2009;110:533–72.
- [36] Rothman LS, Gordon IE, Babikov Y, Barbe A, Benner DC, Bernath PF, et al. The HITRAN 2012 molecular spectroscopic database. *J Quant Spectrosc Radiat Transfer* <http://dx.doi.org/10.1016/j.jqsrt.2013.07.002>, in press.
- [37] Rosenkranz PW. Shape of the 5 mm oxygen band in the atmosphere. *IEEE Trans Antennas Propag* 1975;AP-23:498–506.
- [38] Tran H, Hartmann J-M, Toon G, Brown LR, Frankenberg C, Warneke T, et al. The $2\nu_3$ band of CH_4 revisited with line mixing: consequences for spectroscopy and atmospheric retrievals at $1.67\ \mu\text{m}$. *J Quant Spectrosc Radiat Transfer* 2010;111:1344–56.